Applied Catalysis B: Environmental 146 (2014) 43–49

Contents lists available at ScienceDirect

Applied Catalysis B: Environmental

journal homepage: www.elsevier.com/locate/apcatb

Low-temperature CO oxidation over Co_3O_4-based catalysts: Significant promoting effect of Bi_2O_3 on Co_3O_4 catalyst

Yang Lou, Li Wang*, Zhenyang Zhao, Yanhui Zhang, Zhigang Zhang, Guanzhong Lu, Yun Guo*, Yanglong Guo

Key Laboratory for Advanced Materials, Research Institute of Industrial Catalysis, East China University of Science and Technology, Shanghai, 200237, China

ARTICLE INFO

Article history:
Received 31 October 2012
Received in revised form 5 March 2013
Accepted 11 June 2013
Available online 20 June 2013

Keywords:
Low-temperature CO oxidation
Oxygen vacancy
Co_3O_4
Bi_2O_3
O_2 activation

ABSTRACT

The modification of Co_3O_4 by Bi_2O_3 significantly enhanced its catalytic performance for CO oxidation. The 20 wt.% Bi_2O_3-Co_3O_4 exhibited the best catalytic performance. The results of H_2-TPR and CO-TPR revealed that the mobility of oxygen was accelerated greatly and the ability of low-temperature oxygen activation was the crucial factor to improve the catalytic performance. Bi_2O_3 entered the lattice of Co_3O_4 caused the structural defect and lattice distortion, which should be the origin of the high O_2 activation ability and mobility. Structure-performance correlation demonstrated that the low-temperature oxygen activation was dependent on the defective degree of structure, which was determined by the content of Bi_2O_3. The catalytic behaviors under different reaction conditions revealed that CO could effectively adsorb on the surface active sites and CO_2 could competitively adsorb on the active sites. The ability to supply the active O_2 species was suggested to be a key step. The kinetic data showed not only the amount of surface active sites were increased on the surface of Co_3O_4 but also the catalytic ability of single active site was enhanced greatly.

1. Introduction:

Low-temperature CO oxidation has not only great value on academic but also practical application [1–18]. Among these catalysts, supported noble metal catalysts showed high activity for CO oxidation [1–5]. Although some achievements have been obtained, the high cost of noble metals still inhibited their application. Hence, the study of low-temperature CO oxidation catalyzed by transition metal has been a very important and practical topic.

Co_3O_4 is considered as an alternative to noble metal because of the high activity for low-temperature CO oxidation [6–13]. Co_3O_4 has a spinel structure containing Co^{3+} in an octahedral coordination and Co^{2+} in a tetrahedral coordination [8,10]. Haruta and co-workers [7] reported that Co_3O_4 exhibited excellent low-temperature activity for CO oxidation that T_{50} could be obtained at −54 °C. Thormählen et al. [9] reported that CoO_x/Al_2O_3 could completely convert CO to CO_2 at −43 °C and obtain 50% CO conversion at −63 °C. Xie et al. [10] reported that the Co_3O_4 nanorods with specific morphology mainly exposed [110] plane could catalyze CO oxidation at temperature as low as −77 °C and sustain 100% CO conversion to CO_2 during the initial 6 h.

However, the Co_3O_4 surface was very sensitive to the reaction condition and water concentration. The water was thought to inhibit the O_2 activation [13,14] and the different reaction conditions might influence the accumulation of surface carbonate species [14]. In fact, the good performance of Co_3O_4 catalyst for CO oxidation could be attributed to high activity of lattice oxygen. The experimental and theoretical results [6,7,10–14] indicated that the oxygen activation played a very important role in the reaction processes on the surface of Co_3O_4 and oxygen vacancy was thought to be the best active site for oxygen activation. Hence, it should be a useful method to increase the CO oxidation performance of Co_3O_4 by tuning the amount of surface oxygen vacancy through the pretreatments under different conditions [13], doping the heteroatom in the bulk of Co_3O_4 [6] and etc. In our previous work, the Bi_2O_3 was used to modify the amount of surface oxygen vacancy and the catalytic performance of Co_3O_4 for CO oxidation was enhanced greatly [6].

In our study, we found the modification of Co_3O_4 by Bi_2O_3 could significantly enhance the catalytic performance. This paper would report the catalytic behaviors under different reaction conditions and the effects of Bi_2O_3 on the structural and surface properties of Co_3O_4 catalysts. The reason for the significantly promoted activity of CO oxidation on Bi_2O_3-Co_3O_4 surface was also discussed from perspective of kinetics.

* Corresponding author. Tel.: +86 21 64253703.
E-mail addresses: wangli@ecust.edu.cn (L. Wang), yunguo@ecust.edu.cn (Y. Guo).

0926-3373/$ – see front matter © 2013 Elsevier B.V. All rights reserved.
http://dx.doi.org/10.1016/j.apcatb.2013.06.007

2. Experimental

2.1. Catalyst preparation

The samples were prepared by precipitation and co-precipitation methods. The cobalt acetate ($Co(CH_3COO)_2{\cdot}4H_2O$) and bismuth chloride ($BiCl_3$) were used as precursor salts, and sodium carbonate (Na_2CO_3) was used as precipitant. The preparation method was similar to the reference [10]. 4.98 g cobalt acetate and matching bismuth chloride were dissolved into 80 ml ethylene glycol, and the system was degassed by vacuum. Then the mixture was heated to 160 °C and kept in N_2 flow for 40 min. 200 ml of 0.22 M Na_2CO_3 solution heated at 80 °C was added into the above solution prepared, and mixture was further aged at 160 °C for 1 h under vigorously stirring. The precipitate was washed using distilled water until no Cl^- was detected by $AgNO_3$ solution. After filtering, the solid powder obtained was dried at 65 °C overnight and calcined at 350 °C for 4 h in air. The calculated contents of Bi_2O_3 were 15, 18, 20, 22 and 25 wt.%.

2.2. Evaluation of the catalytic performance

The activity of catalysts for CO oxidation was evaluated in a fixed-bed reactor at atmospheric pressure, and 200 mg catalyst (40–60 mesh) was used. The feed gas of 1 vol.% CO and 20 vol.%O_2 in N_2 passed through the catalytic bed at a flow rate of 50 ml/min. Before the experiments, the catalyst was pretreated at 350 °C for 40 min in 20 vol.% O_2/N_2 (50 ml/min). The dry feed gas was obtained by passing the feed gas through molecular-sieve trap cooled to −80 °C. The conversion of CO was measured from room temperature to the temperature of CO conversion below 20%. The temperature was adjusted by using ethanol and liquid nitrogen mixture. The concentrations of CO and CO_2 in the outlet stream were measured by an on-line gas chromatograph after the catalyst bed temperature was stabilized at the settled value for 15 min to obtain the steady state. For testing the effects of preadsorption, the procedures were followed: the gas (CO, O_2 and CO_2) was preadsorbed for 15 min, then the catalytic activity was tested as described at above and the feed gas was 1 vol.% CO, 20 vol.% O_2 and N_2 balanced.

2.3. Catalyst characterization

2.3.1. CO-TPR

The temperature-programmed reduction of CO (CO-TPR) was performed under a flow of 5 vol.% CO/N_2 (50 ml/min) over 200 mg catalyst using a heating rate of 10 °C/min. Before CO-TPR experiment, the samples were pretreated using 20 vol.% O_2/N_2 (50 ml/min) mixed gas at 350 °C for 40 min. A mass spectrometer (MS, ICP 400, INFICON, Co. Ltd.) was used for monitoring the effluent gas. The mass signal of CO_2 (m/z = 44) was recorded. For the low temperature CO-TPR, the sample was cooled to -80 °C and then adsorbed CO for 1 h. The blank experiment was carried on with the same procedure in the flow of pure N_2.

2.3.2. H_2-TPR

The temperature-programmed reduction of H_2 (H_2-TPR) was performed with a commercial temperature-programmed system. 50 mg of the catalyst was heated in the flow of 5 vol.% H_2/N_2 (20 ml/min) at a heating rate of 10 °C/min from −80 °C to room temperature (Low-temperature H_2-TPR) or from room temperature to 850 °C (High-temperature H_2-TPR). The amount of H_2 uptake during the reduction was measured by thermal conductivity detector (TCD). Before H_2-TPR experiment, the samples were pretreated by 20 vol.% O_2/N_2 (50 ml/min) mixed gas at 350 °C for 40 min.

2.3.3. XRD

In order to get the information about the structure of the samples, the XRD spectra were obtained with Rigaku D/max 2550 VB/PC diffractometer using a Cu Kα radiation (λ = 1.54056 Å). The X-ray tube was operated at 40 kV and 100 mA. The intensity data was collected at room temperature in a 2θ range from 10° to 80° with a scan rate of 6°/min.

2.3.4. BET

The BET surface areas were measured by nitrogen adsorption at liquid nitrogen temperature by using a surface area and porosity analyzer (Quantachrome NOVA 4000e apparatus). Before measurement, the samples were degassed at 180 °C for 6 h in vacuum.

2.3.5. Raman

Raman spectra was recorded with thin wafer on a Renishaw spectrometer by using a 514 nm Ar^+ laser as the excitation source at room temperature. The laser beam intensity and the spectrum slit width were 2 mW and 3.5 cm^{-1}, respectively.

2.3.6. Kinetic measurements

The kinetic measurements were carried out in the temperature range of −55 °C to −102 °C and space velocity of 40,000–600,000 ml/g h with feed steams of 0.2–2 vol.% CO and 5–20 vol.% O_2, balanced with N_2, to make sure the CO conversion was below 15% so as to eliminate the thermal effect and diffusion effect before calculating the reaction rates.

2.3.7. O_2-TPD

The temperature-programmed desorption of O_2 (O_2-TPD) was performed from -80 °C to room temperature. The procedures were as followed: (1) the sample was pretreated under 20 vol.% O_2/N_2 (50 ml/min) mixed gas at 350 °C for 40 min; (2) the sample was cooled to −80 °C and sustained O_2 adsorption for 1 h; (3) the sample was purged with He for 1 h; (4) the sample was heated at a rate of 10 °C/min from −80 °C to room temperature. The signal of O_2 desorption from the sample was measured by thermal conductivity detector (TCD).

3. Results

3.1. The effects of Bi_2O_3 content on catalytic performance of the Bi_2O_3-modified Co_3O_4 catalysts

The effects of Bi_2O_3 contents on the catalytic activity of Co_3O_4 catalysts were shown in Fig. 1. Only 10% conversion of CO could be obtained on the pure Bi_2O_3 at room temperature. For pure Co_3O_4, the lowest temperature of complete conversion (LTCC) of CO was −40 °C. The doping of Bi_2O_3 on Co_3O_4 could greatly enhance the CO oxidation and the amount of Bi_2O_3 showed great effect on the catalytic activity and stability. However, the excessive amount of Bi_2O_3 did not further promote the catalytic activity of Co_3O_4.

Table 1
The LTCC, Reaction rate and TOF of different Bi_2O_3-Co_3O_4 catalysts for CO oxidation.

Bi_2O_3 content (wt.%)	LTCC[a] (°C)	Reaction rate[b] (μmol g^{-1} s^{-1})	TOF[c] (10^{-8} mol/s m^2)
0	−40	3.89	3.2
15	−86	11.74	8.0
20	−89	17.05	12.8
25	−58	7.89	6.0

[a] LTCC: the lowest temperature of complete conversion
[b] Reaction rate: measured at −75 °C under reaction condition of 2 vol.% CO, 10 vol.% O_2, N_2 balance with SV = 600,000 ml/g h.
[c] TOF values were calculated based on the BET surface area not on the amount of surface active sites.

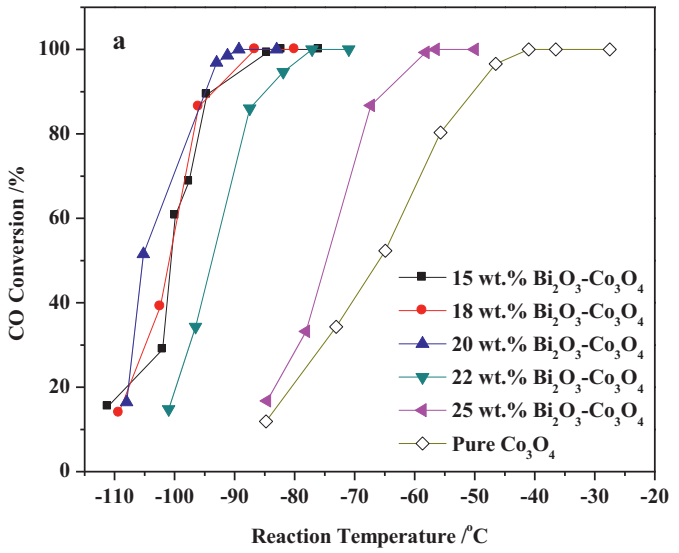

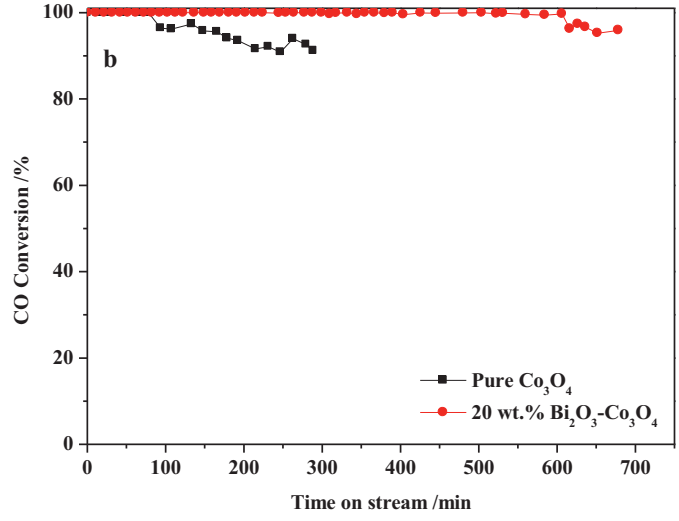

Fig. 1. The catalytic activities of Bi_2O_3-Co_3O_4 samples for CO oxidation (a) and The catalytic stability of pure Co_3O_4 was measured at −40 °C and 20 wt.% Bi_2O_3-Co_3O_4 was measured at −75 °C under dry condition (b).

20 wt.% Bi_2O_3-Co_3O_4 exhibited the highest catalytic activity and the LTCC of CO was −89 °C. Compared with the pure Co_3O_4, the reaction rate of Bi_2O_3-Co_3O_4 samples was increased greatly from the kinetic data showed in the Table 1. Especially, the reaction rate of 20 wt.% Bi_2O_3-Co_3O_4 was about 4.4 times to that of Co_3O_4. At the same time, the stability of Co_3O_4 was enhanced greatly. Under dry feed gas condition, the complete CO conversion was sustained at −40 °C for 80 min over pure Co_3O_4, while 20 wt.% Bi_2O_3-Co_3O_4 could completely oxidize CO at −75 °C for 600 min.

3.2. Catalytic behaviors of 20 wt.% Bi_2O_3-Co_3O_4 catalysts under different reaction conditions.

3.2.1. The effect of CO concentration on the catalytic activity of 20 wt.% Bi_2O_3-Co_3O_4

The CO concentration had great effect on the activity of 20 wt.% Bi_2O_3-Co_3O_4 as shown in Fig. 2. The catalyst exhibited much better activity under lower CO concentration condition. The CO could be completely converted even at -108 °C when the CO concentration was decreased to 0.5 vol.%. But when increasing CO concentration to 2 vol.% and pre-adsorbing CO on the surface, the LTCC was

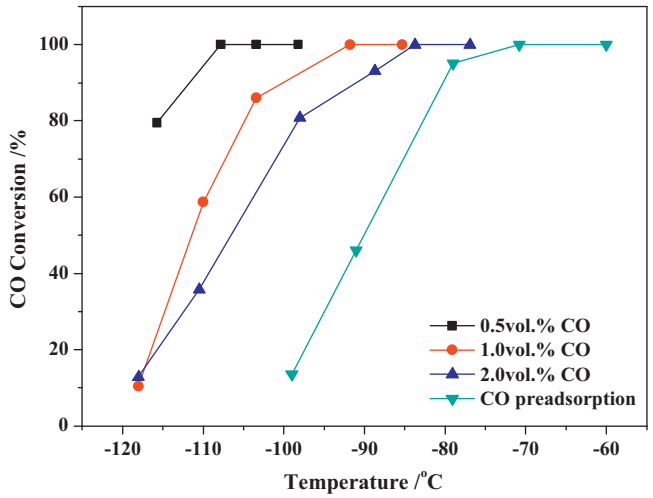

Fig. 2. The effects of CO concentration and pre-adsorption on the activity of 20 wt.% Bi_2O_3-Co_3O_4.

decreased to −84 °C and −70 °C. These results indicated that preadsorbed CO could occupy the active sites and inhibit the adsorption and dissociation of O_2. For the higher CO concentration, the supply of active oxygen might not match the consumption of adsorbed CO, which decreased the activity for CO oxidation.

3.2.2. The effect of O_2 concentration on the catalytic activity of 20 wt.% Bi_2O_3-Co_3O_4

The oxygen played an important role in CO oxidation over Co_3O_4 catalysts. As shown in Fig. 3, increasing the oxygen concentration could significantly improve the catalytic activity. When the O_2 concentration was up to 30 vol.%, CO could be completely converted to CO_2 at as low as −105 °C and 50% CO conversion was obtained even at −115 °C. Moreover, the pre-adsorption of O_2 also obviously promoted the catalytic activity and the LTCC could be obtained at −106 °C. The catalytic activity was the worst when the O_2 concentration was 10 vol.%.

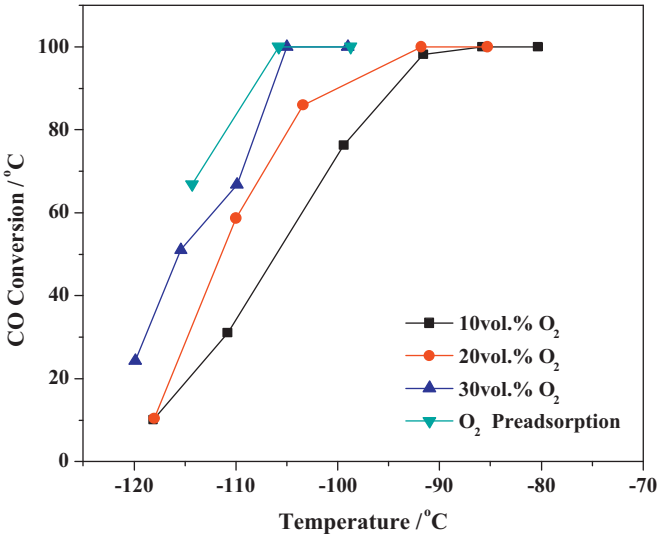

Fig. 3. The effects of oxygen concentration and oxygen pre-adsorption on the catalytic activity of 20 wt.% Bi_2O_3-Co_3O_4.

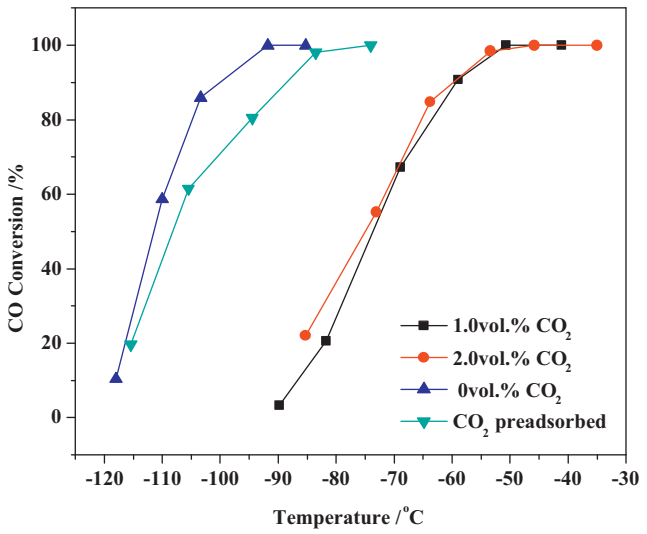

Fig. 4. The effects of CO_2 concentration and pre-adsorption on the catalytic activity of 20 wt.% Bi_2O_3-Co_3O_4.

3.2.3. The effect of CO_2 concentration on the catalytic activity of 20 wt.% Bi_2O_3-Co_3O_4

For investigating the influence of reaction product on the catalytic reaction, the effect of CO_2 was studied as shown in Fig. 4. The presence of CO_2 in the feed stream obviously inhibited the CO oxidation on 20 wt.% Bi_2O_3-Co_3O_4. The LTCC increased from −89 °C to −51 °C when adding 1 vol.% CO_2 into the feed gas. The activity didn't further decrease with the increase of CO_2 concentration. And the LTCC of 20 wt.% Bi_2O_3-Co_3O_4 was raised to −74 °C after pre-adsorbing CO_2. These results implied that the CO_2 molecule might competitively adsorb on the active sites with the reactants and inhibit the adsorption of reactants.

3.3. Structural characteristics of the Co_3O_4 catalysts modified by Bi_2O_3

3.3.1. Surface area and crystalline structure

XRD patterns of different Bi_2O_3-Co_3O_4 catalysts were shown in Fig. 5. For the Bi_2O_3-Co_3O_4, the characteristic peak of Bi_2O_3 was observed at about 32.8°. And the diffraction peaks of Co_3O_4 shifted to lower 2θ degree slightly. It indicated that the Bi^{3+} inserted the lattice of Co_3O_4 during the preparation process, and the lattice parameter of Co_3O_4 was changed due to the unmatched larger radius of Bi^{3+} (r = 0.103 nm). At the same time, the characteristic peak of Co_3O_4 became broad obviously after the deposition of Bi_2O_3, which revealed the reduction of crystalline size. The crystal sizes of Bi_2O_3-Co_3O_4 samples calculated based on Scherrer Equation were similar, but smaller than that of pure Co_3O_4 (7.3 nm) shown in Table 2. The results indicated that the insertion of Bi_2O_3 induced the structural change of Co_3O_4 and suppressed the growth of crystal.

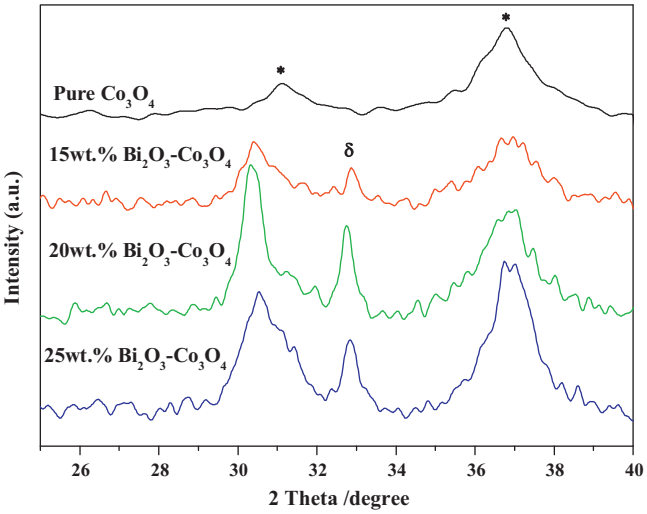

Fig. 5. XRD patterns of Bi_2O_3-Co_3O_4 samples, *: Co_3O_4 phase; δ: Bi_2O_3 phase.

Table 2
BET surface areas and crystal sizes of Co_3O_4 samples doped by different Bi_2O_3 contents.

Bi_2O_3 content (wt.%)	0	15	20	25
BET (m^2/g)	121.6	147.3	133.6	132.2
Crystal size (nm)	7.3	5.0	5.4	5.5

3.3.2. Structural defects of the Bi_2O_3-Co_3O_4 catalysts

Fig. 6 showed the Raman spectra of Bi_2O_3-Co_3O_4 samples and pure Co_3O_4. For pure Co_3O_4, five Raman peaks at 191, 481, 524, 617 and 688 cm^{-1} were observed corresponding to the $F_{2g}^{(1)}$, E_g, $F_{2g}^{(2)}$, $F_{2g}^{(3)}$ and A_{1g} symmetry of Co_3O_4 [19–21], respectively. Bi_2O_3-Co_3O_4 samples gave the similar Raman spectra with Co_3O_4, while the characteristic peaks of Bi_2O_3 could not be detected [22,23]. Compared with Co_3O_4, all of the Raman peaks on Bi_2O_3-Co_3O_4 samples shifted to the lower frequencies and broadened, which was associated with the lattice distortion or residual stress of the spinel structure [24]. The results of XRD and Raman spectra showed that 20 wt.% Bi_2O_3-Co_3O_4 exhibited the maximum structural defects, which was in line with 20 wt.% Bi_2O_3-Co_3O_4 owning the highest catalytic activity.

3.4. Reducibility of the Bi_2O_3-Co_3O_4 catalysts

3.4.1. H_2-TPR

The high-temperature H_2-TPR profiles of pure Co_3O_4, pure Bi_2O_3 and Bi_2O_3-Co_3O_4 samples were shown in Fig. 7(a). The TPR of Bi_2O_3 showed a broad reduction peak at the temperature range of 350–600 °C. Three reduction peaks were observed on Co_3O_4, which corresponded to the reduction of surface oxygen species (130 °C), the reduction of Co^{3+} to Co^{2+} (α_1), and the reduction of Co^{2+} to Co^0 (α_2), respectively [25–29].

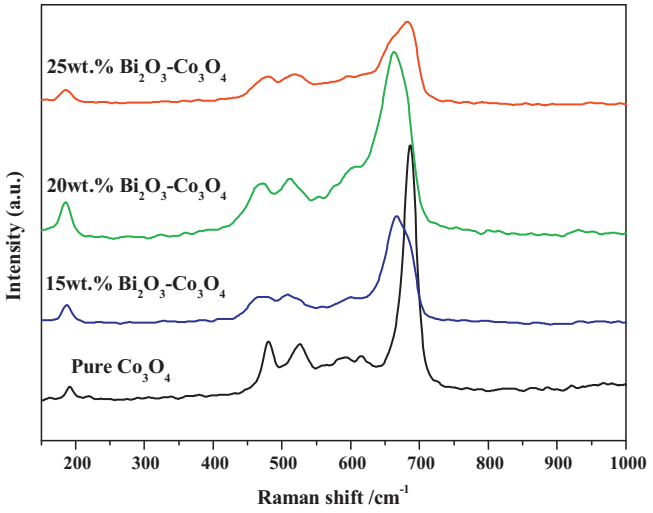

Fig. 6. Raman spectra of 15 wt.% Bi_2O_3-Co_3O_4, 20 wt.% Bi_2O_3-Co_3O_4, 25 wt.% Bi_2O_3-Co_3O_4 and Co_3O_4.

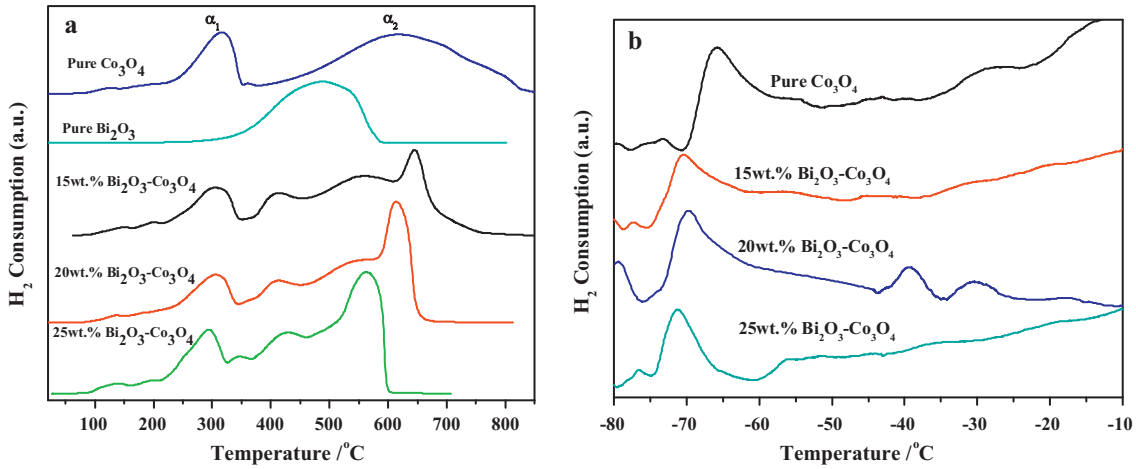

Fig. 7. High-temperature (a) / Low-temperature (b)-H_2-TPR profiles of pure Co_3O_4 and Bi_2O_3-Co_3O_4 samples.

Compared with the pure Co_3O_4, the reduction of Bi_2O_3-Co_3O_4 samples became more complex. The new peak in the temperature range of 360 to 460 °C could be ascribed to the reduction of Bi_2O_3. The reduction peaks in the temperature range of 450 to 700 °C, including a weak broad peak and a sharp reduction peak, could be attributed to the reduction of Co^{2+}. The reduction of Co^{3+} (α_1) and Co^{2+} (α_2) shifted to lower temperature after the deposition of Bi_2O_3. The sharp reduction peak, attributed to the reduction of Co^{2+}, implied that the oxygen diffusion in bulk Co_3O_4 was accelerated significantly.

The low-temperature H_2-TPR profiles of pure Co_3O_4 and Bi_2O_3-Co_3O_4 samples showed in the Fig. 7 (b). There was an obvious reduction peak at −60 °C on pure Co_3O_4 and obvious reduction peak at around −70 °C on the Bi_2O_3-Co_3O_4 samples. However, there was another obvious peak at −80 °C on the 20 wt.% Bi_2O_3-Co_3O_4. Continuously increasing the content of Bi_2O_3 to 25%, the reduction peak at −80 °C disappeared. The 20 wt.% Bi_2O_3-Co_3O_4 showed the best reducibility, which was in accordance with its highest catalytic activity. These results revealed the doping of Bi_2O_3 promoted the reducibility and oxygen mobility of Co_3O_4 and enhanced the CO oxidation activity.

3.4.2. CO-TPR

The low-temperature CO-TPR of pure Co_3O_4 and 20 wt.% Bi_2O_3-Co_3O_4 were showed in Fig. 8. The lattice oxygen on surface layer was regarded as playing an important role in this reduction reaction [30–34]. Two obvious CO consumption peaks could be observed on 20 wt.% Bi_2O_3-Co_3O_4 at the temperature range of −80 to −20 °C, which was ascribed to the contribution of surface highly active lattice oxygen or weakly adsorbed molecular oxygen species. However, the CO consumption was obviously detected over pure Co_3O_4 only at the temperature higher than −20 °C, which indicated that the activation of lattice oxygen was accelerated significantly on 20 wt.% Bi_2O_3-Co_3O_4 due to the structural defects and the interaction between Bi_2O_3 and Co_3O_4.

3.4.3. Low-temperature O_2-TPD

To further investigate the adsorption and activation of oxygen on the surface of Co_3O_4-based catalysts, low-temperature O_2-TPD experiments were carried out from −80 °C to 0 °C, the results were shown in the Fig. 9. An obvious O_2 desorption peak was observed in the temperature range of −75 to −50 °C. The desorption peak of the Co_3O_4-based catalysts could be attributed to the molecular oxygen species adsorbed on the oxygen vacancy [13]. The nature of the active site of the catalyst could be evaluated by the difference of the amount of the active sites and the intrinsic activity of the active sites [17]. For the Bi_2O_3-Co_3O_4 samples, the O_2 desorption peak gradually shifted to the lower temperature with the increasing of Bi_2O_3 contents, meanwhile, the desorption amount of O_2 increased. For example, the desorption amount of O_2 on 20 wt.% Bi_2O_3-Co_3O_4 -Co_3O_4 was 1.76 times of that on pure Co_3O_4. However, the O_2 desorption peak shifted to higher temperature with continuously increasing the Bi_2O_3 contents to 25%, and the amount of desorbed O_2 decreased about 8%.

3.5. Reaction order and apparent activation energy

The kinetic data was showed in the Fig. 10. The apparent activation energy calculated were 19.0 kJ mol^{-1} and 20.1 kJ mol^{-1} for 20 wt.% Bi_2O_3-Co_3O_4 and pure Co_3O_4 as shown in Fig. 10 (a), which was in line with the previous data [10,13]. The reaction orders of CO and O_2 shown in Fig. 10 (b) were −1.54 and 0.65 over the 20 wt.% Bi_2O_3-Co_3O_4 and −0.84 and 1.02 over pure Co_3O_4, respectively.

4. Discussion

Our results showed that Bi_2O_3-Co_3O_4 samples exhibited much higher catalytic activity than pure Co_3O_4 and 20 wt.% Bi_2O_3-Co_3O_4

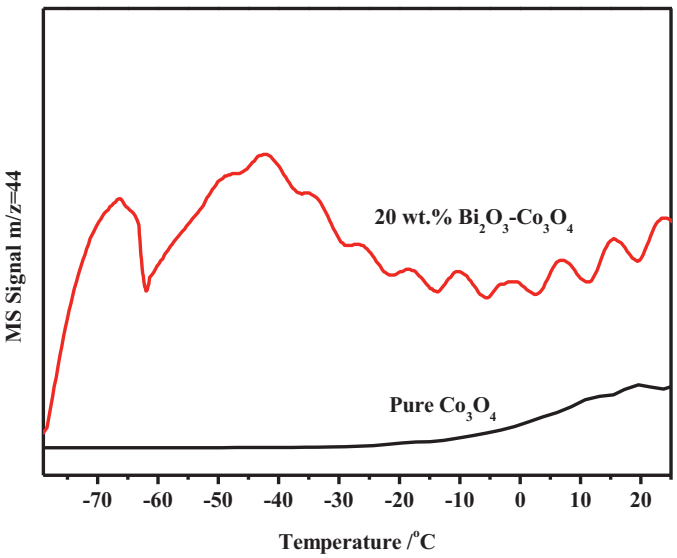

Fig. 8. Low-temperature CO-TPR profiles of 20 wt.% Bi_2O_3-Co_3O_4 and Co_3O_4.

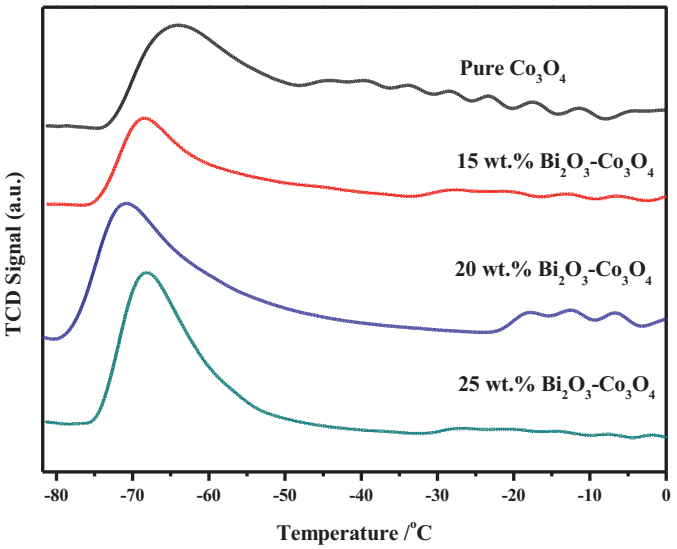

Fig. 9. Low-temperature O_2-TPD of pure Co_3O_4 and Bi_2O_3-Co_3O_4 samples.

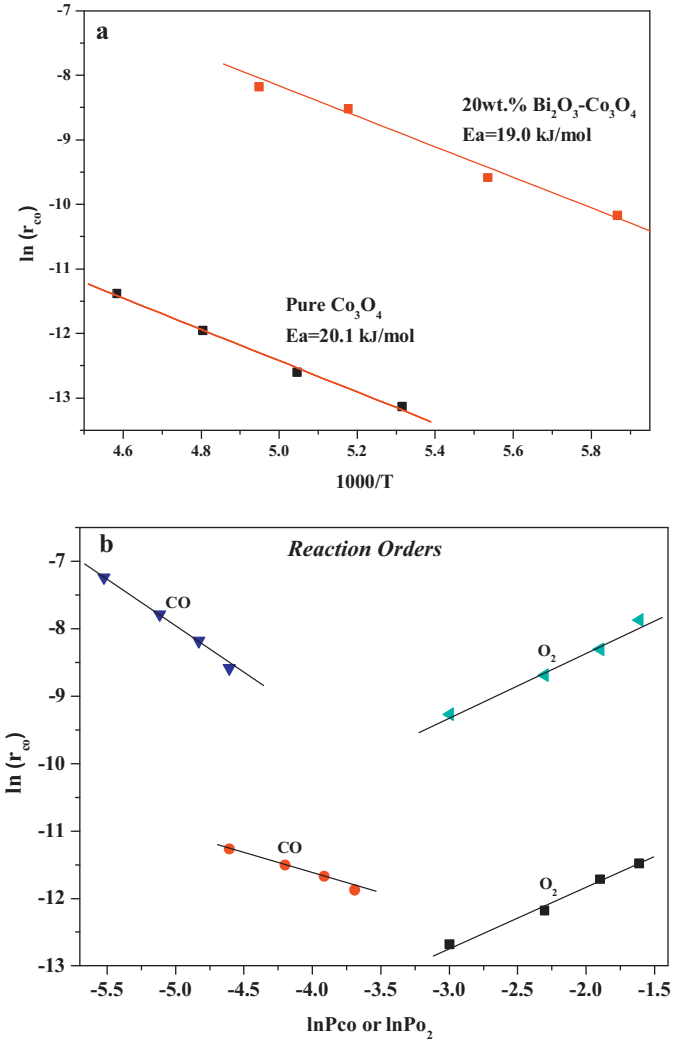

Fig. 10. The kinetic data of pure Co_3O_4 and 20 wt.% Bi_2O_3-Co_3O_4: Activation energy (a), Reaction order of pure Co_3O_4 and 20 wt.% Bi_2O_3-Co_3O_4 (b), (●) CO over pure Co_3O_4; (■) O_2 over pure Co_3O_4; (▼) CO over 20 wt.% Bi_2O_3-Co_3O_4; (◄) O_2 over 20 wt.% Bi_2O_3-Co_3O_4.

showed the best catalytic activity. However, the excessive Bi_2O_3 (25 wt.%) did not further improve the activity of Co_3O_4.

As we know, for the CO oxidation over Co_3O_4 catalysts, CO firstly adsorbed on the Co^{3+}, then the adsorbed CO reacted with the lattice oxygen to produce CO_2 and oxygen vacancy. The oxygen vacancy would be replenished by O_2 to form the new active oxygen species and complete the redox cycle [10,14]. Therefore, the activity of lattice oxygen and the activation of gas O_2 played an important role in the CO oxidation.

The results of XRD and Raman confirmed that the structural defects and distortion induced by the insertion of Bi^{3+} into the lattice of Co_3O_4 and the interaction between Bi_2O_3 and Co_3O_4. The significant Bi_2O_3 phase was observed in Bi_2O_3-Co_3O_4 samples and the diffraction peaks of Bi_2O_3 increased with increasing the Bi_2O_3 contents from 15 wt.% to 20 wt%. However, the diffraction peaks of 25 wt.% Bi_2O_3-Co_3O_4 did not show the further shift of Co_3O_4, and the peak intensity of Bi_2O_3 did not enhance as expected. Combined with the results of Raman, it was implied that the introduction of 20 wt.% Bi_2O_3 in Co_3O_4 produced the maximum structural defects, and the excessive Bi_2O_3 could not aggravate the structural defect and lattice distortion.

The structural defects and lattice distortion could promote the formation of oxygen vacancy, which was beneficial for the activation and mobility of oxygen. The H_2-TPR and CO-TPR results showed that the activation and mobility of lattice oxygen were accelerated on Bi_2O_3-Co_3O_4, which meant the ability of supplying active oxygen was enhanced greatly after the deposition of Bi_2O_3. O_2-TPD results also indicated that the ability of O_2 adsorption on the Bi_2O_3-Co_3O_4 was enhanced. At the same time, the effects of CO and O_2 concentration on the activity showed the supplying of active oxygen species played a very important role in the CO oxidation over Co_3O_4-based catalyst. Hence, the structural defects of Co_3O_4 induced by the insertion of Bi^{3+} and the interaction between Bi_2O_3 and Co_3O_4 were suggested to be the origin of the high abilities for the activation and mobility of O_2. The formation of a thin layer of inactive Bi_2O_3 on the surface was also probably reduced the activity of 25 wt.% Bi_2O_3-Co_3O_4 for CO oxidation.

The kinetic data showed that the activation energy of pure Co_3O_4 (20.1 kJ mol^{-1}) was almost same as that of 20 wt.% Bi_2O_3-Co_3O_4 sample (19.0 kJ mol^{-1}). However, the pre-exponential factor of 20 wt.% Bi_2O_3-Co_3O_4 was about 32 times to that of pure Co_3O_4. Xie et al. [10] reported that the increase on the pre-exponential factor stood for the increase on the amount of active sites on the Co_3O_4 for CO oxidation. Hence, it was clear that the amount of active sites on 20 wt.% Bi_2O_3-Co_3O_4 increased obviously compared with that on pure Co_3O_4.

At the same time, the reaction rates of Bi_2O_3-Co_3O_4 samples were obviously higher than that of Co_3O_4 under the same reaction condition. For example, the TOF on 20 wt.% Bi_2O_3-Co_3O_4 was about 4.4 times to that on Co_3O_4. The reaction orders of CO on 20 wt.% Bi_2O_3-Co_3O_4 were lower (−1.54) than that of Co_3O_4 (−0.84), which indicated the CO adsorption on 20 wt.% Bi_2O_3-Co_3O_4 was stronger than that on Co_3O_4 [35]. However, the reaction orders of O_2 on 20 wt.% Bi_2O_3-Co_3O_4 and Co_3O_4 showed different trends, 0.65 on 20 wt.% Bi_2O_3-Co_3O_4 catalyst and 1.02 on pure Co_3O_4 which suggested the adsorption and activation of O_2 over 20 wt.% Bi_2O_3-Co_3O_4 was easier than that over pure Co_3O_4 [13]. These results indicated that the doping of Bi_2O_3 not only increased the amount of active sites but also promoted the catalytic ability of active sites.

5. Conclusions

The Bi_2O_3-Co_3O_4 showed high catalytic activity for low-temperature CO oxidation. Under dry feed gas condition, the 20 wt.% Bi_2O_3-Co_3O_4 showed the best catalytic performance and

CO could be completely converted to CO_2 at as low as −89 °C and sustain the complete conversion at −75 °C for 600 min. But the excessive doped content of Bi_2O_3 inhibited the catalytic activity. The redox ability of Co_3O_4 was significantly promoted by the structure defects and the interaction between Bi_2O_3 and Co_3O_4, which promoted the activation and the mobility of active oxygen species. The kinetic data suggested the ability to provide the active O_2 species should be a key step. The modification of Co_3O_4 by Bi_2O_3 increased the amount of surface active sites, and enhanced the adsorption of CO and activation of O_2.

Acknowledgements

This project was supported financially by the National Basic Research Program of China (2010CB732300, 2013CB933201), the National High Technology Research and Development Program of China (2011AA03A406), National Natural Science Foundation of China (21171055), and the New Century Excellent Talents in University (NECT-10-0377).

References

[1] S.A.C. Carabineiro, B.F. Machado, R.R. Bacsab, P. Serpb, G. Dražić, J.L. Faria, J.L. Figueiredo, J. Catal. 273 (2010) 191.
[2] S.Y. Li, G. Liu, H.L. Lian, M.J. Jia, G.M. Zhao, D.Z. Jiang, W.X. Zhang, Catal. Commun. 9 (2008) 1045.
[3] M. Haruta, T. Kobayashi, N. Yamada, Chem. Lett. 16 (1987) 405.
[4] M.S. Chen, D.W. Goodman, Science 306 (2004) 252.
[5] B.T. Qiao, L.Q. Liu, J. Zhang, Y.Q. Deng, J. Catal. 261 (2009) 241.
[6] Y. Lou, L. Wang, Y.H. Zhang, Z.Y. Zhao, Z.G. Zhang, G.Z. Lu, Y. Guo, Catal. Today 175 (2011) 610.
[7] D.A.H. Cunningham, T. Kobayashi, N. Kamijo, M. Haruta, Catal. Lett. 25 (1994) 257.
[8] Y.Z. Wang, Y.X. Zhao, C.G. Gao, D.S. Liu, Catal. Lett. 116 (2007) 136.
[9] P. Thormählen, M. Skoglundh, E. Fridell, B. Andersson, J. Catal. 188 (1999) 300.
[10] X.W. Xie, Y. Li, Z.Q. Liu, M. Haruta, W.J. Shen, Nature 458 (2009) 746.
[11] J. Jansson, A.E.C. Palmqvist, E. Fridell, M. Skoglundh, L. Österlund, P. Thormählen, V. Langer, J. Catal. 211 (2002) 387.
[12] J. Jansson, J. Catal. 194 (2000) 55.
[13] Y.B. Yu, T. Takei, H. Ohashi, H. He, X.L. Zhang, M. Haruta, J. Catal. 267 (2009) 121.
[14] H.F. Wang, R. Kavanagh, Y.L. Guo, Y. Guo, G.Z. Lu, P. Hu, Angew. Chem. Int. Ed. 51 (2011) 6657.
[15] J. Xu, T. White, P. Li, C.H. He, J.G. Yu, W.K. Yuan, Y.F. Han, J. Am. Chem. Soc. 132 (2010) 10398.
[16] M.S. Chen, D. Kumar, C.W. Yi, D.W. Goodman, Science 310 (2005) 291.
[17] Y. Liu, C. Wen, Y. Guo, G.Z. Lu, Y.Q. Wang, J. Phys. Chem. C 114 (2010) 9889.
[18] S. Kunz, F.F. Schweinberger, V. Habibpour, M. Röttgen, C. Harding, M. Arenz, U. Heiz, J. Phys. Chem. C 114 (2010) 1651.
[19] L. He, Z.C. Li, Z.J. Zhang, Nanotechnology 19 (2008) 155606.
[20] V.G. Hadjievl, M.N. Ilievl, I.V. Vergilov, J. Phys. C: Solid State Phys. 21 (1988) l99.
[21] Q. Liu, L.C. Wang, M. Chen, Y. Cao, H.Y. He, K.N. Fan, J. Catal. 263 (2009) 104.
[22] S.N. Narang, N.D. Patel, V.B. Kartha, J. Mol. Struct. 327 (1994) 221.
[23] M. Prekajski, A. Kremenović, B. Babić, M. Rosić, B. Matović, A.R. Mihajlović, M. Radović, Mater. Lett. 64 (2010) 2247.
[24] I. Lopes, N.E. Hassan, H. Guerba, G. Wallez, A. Davidson, Chem. Mater. 18 (2006) 5826.
[25] L. Xue, C.B. Zhang, H. He, Y. Teraoka, Appl. Catal. B 75 (2007) 167.
[26] P.G. Harrison, I.K. Ball, W. Daniell, P. Lukinskas, M. Céspedes, E.E. Miró, M.A. Ulla, Chem. Eng. J. 95 (2003) 47.
[27] N. Bahlawane, E.F. Rivera, K.K. Höinghaus, A. Brechling, U. Kleineberg, Appl. Catal. B 53 (2004) 245.
[28] H.Y. Lin, Y.W. Chen, Mater. Chem. Phys. 85 (2004) 171.
[29] B. Mazumder, J.C. Védrine, Appl. Catal. A: Gen. 245 (2003) 87.
[30] L.F. Liotta, G.D. Carlo, G. Pantaleo, G. Deganello, Catal. Commun. 6 (2005) 329.
[31] H.F.J. van't Blik, R. Prins, J. Catal. 97 (1986) 188.
[32] A.A. Yaremchenko, V.V. Kharton, S.A. Veniaminov, V.D. Belyaev, V.A. Sobyanin, F.M.B. Marques, Catal. Commun 8 (2007) 335.
[33] M.V.D. Bossche, S.J. McIntosh, J. Catal. 255 (2008) 313.
[34] L.H. Hu, K.Q. Sun, Q. Peng, B.Q. Xu, Y.D. Li, Nano Res. 3 (2010) 363.
[35] M.M. Schubert, M.J. Kahlich, H.A. Gasteiger, R.J. Behm, J. Power Sources 8 (1999) 175.